Materials Chemistry and Physics 319 (2024) 129295

Contents lists available at ScienceDirect

Materials Chemistry and Physics

journal homepage: www.elsevier.com/locate/matchemphys

# Enhancing thermoelectric properties of multilayer graphene with Au deposition

Dwi Nugraheni Rositawati [a,b], Eri Widianto [b,c], Suprapto [d], Tjipto Sujitno [d], Moh. Adhib Ulil Absor [b], Sholihun [b], Kuwat Triyana [b], Iman Santoso [b,*]

[a] Department of Physics Education, Faculty of Teacher Training and Education, Sanata Dharma University, Jl. Affandi Mrican Tromol Pos 29, Yogyakarta, 55002, Indonesia
[b] Department of Physics, Faculty of Mathematics and Natural Sciences, Universitas Gadjah Mada, Sekip Utara PO Box BLS 21, Yogyakarta, 55281, Indonesia
[c] Department of Physics, Faculty of Engineering, Universitas Singaperbangsa Karawang, Telukjambe Timur, Karawang, 41361, Indonesia
[d] Research Center for Accelerator Technology, Nuclear Energy Research Organization, National Research and Innovation Agency (BRIN), Jl. Puspiptek Kec. Setu, Kota Tangerang Selatan , Banten, 15314, Indonesia

## HIGHLIGHTS

- Multilayer graphene with Au deposited was conducted to enhance the thermoelectric properties.
- The Seebeck coefficient, power factor, and resistivity are analyzed.
- The maximum Seebeck coefficient obtained was 4.67 μV/K at 528 K, compared to 0.66 μV/K for pristine graphene.
- An increasing $I_D/I_G$ ratio led to a 24-fold increase in the power factor compared to pristine graphene.
- All samples exhibited p-type conduction, where the dominant charge carriers are holes.

## ARTICLE INFO

*Keywords:*
Au deposited
Seebeck coefficient
Power factor
Graphene

## ABSTRACT

This study examines the effect of Au deposition on the thermoelectric properties of multilayer CVD graphene films. The Raman spectra show that Au deposition impacts the morphology as well as the thermoelectric properties of multilayer CVD graphene films. The D band and G band intensity ratio ($I_D/I_G$) increases according to increasing the concentration of Au, while the 2D band and G band intensity ratio ($I_{2D}/I_G$) ratio decreases. An increasing in the Seebeck coefficient and power factor associated with an increasing in the formation of structural defects in the sample. The maximum Seebeck coefficient obtained was around 4.67 μV/K compared to 0.66 μV/K for pristine graphene at 528 K. Our findings suggest that Au-deposited graphene provides insight into the fundamental study of physics that controls thermoelectric properties the thermoelectric properties of Au-deposited graphene materials.

## 1. Introduction

Due to its ability to generate electricity from heat directly, thermoelectric materials are generating more interest [1–3]. The utilization of waste heat without a combustion reaction has aroused the curiosity of many researchers interested in converting heat into electricity [4,5]. The figure of merit ($ZT$) provides a typical way to describe conversion efficiency, denoted as $ZT = \sigma^2 ST/\kappa$, where $\sigma$ is electrical conductivity, $S$ is the Seebeck coefficient, $T$ is temperature, and $\kappa$ is thermal conductivity. Recent developments in the field of thermoelectric research encompass the novelty discovery of high-performing thermoelectric materials and the optimization of their efficiency through manipulating their structure [6,7], doping [8], band engineering, and nanostructures [9]. Thermoelectric materials possess potential applications in diverse sectors such as automotive, aerospace, and electronics, where they can harness exhaust heat to power sensors and other devices [7,10]. The progressions present possibilities for developing energy technologies that are both more efficient and environmentally conscious.

Several methods have been proposed to enhance the $ZT$ of recently discovered materials in the past few decades. These strategies can be

* Corresponding author.
*E-mail address:* iman.santoso@ugm.ac.id (I. Santoso).

https://doi.org/10.1016/j.matchemphys.2024.129295
Received 7 October 2023; Received in revised form 4 February 2024; Accepted 3 April 2024
Available online 3 April 2024

loosely categorized into two main groups: structural and stain engineering. Structural engineering can be used to increase phonon scattering so that the lattice thermal conductivity decreases. Utilizing structural engineering allows for the reduction of lattice thermal conductivity by enhancing phonon scattering mechanisms. This strategy elevates the presence scattering of phonons sites by introducing dislocations, point defects, and grain boundaries to increase the Seebeck coefficient (*S*) [7–9,11]. Strain engineering induces localized higher band degeneration in order to enhance the Seebeck coefficient (*S*) [12], while atomic deformation is utilized to separate phonon-electron transports, leading to improved carrier mobility [13,14]. These strategies aim to optimize the concentration of carriers, either electrons or holes, through processes such as alloying and doping [15–17].

Two-dimensional semiconductor materials exhibit improved thermoelectric capabilities. These materials demonstrate robust electrical conductivity, impressive mechanical characteristics, and notable resistance to environmental factors. Graphene, an atomically thin 2D carbon allotrope, exhibits remarkable attributes, including excellent electrical and thermal conductivity, high transparency, an inherent absence of a bandgap, and a semi-metallic nature [18–20]. Altering graphene structures through methods such as hydrogenation, doping, and patterning allows for preserving its exceptional characteristics while also customizing or enhancing specific properties to suit diverse applications [21–26]. The remarkably elevated thermal conductivity of pristine graphene (5000 W/mK) offers an effective solution for managing heat in nanoelectronic devices [27,28], and its exceptional mechanical characteristics suggest the potential for developing flexible electronics based on graphene [21,29]. However, the thermoelectric effectiveness of graphene falls short of practical application as a thermoelectric material, mostly because of its outstanding heat conduction properties [30,31].

Furthermore, the absence of a bandgap in the electronic band structure of graphene leads to contrasting contributions from electrons and holes. As a result, graphene encounters challenges in maintaining a substantial concentration of a single carrier type, resulting in a diminished Seebeck coefficient [32,33]. Two approaches for improving the thermoelectric efficiency of graphene involve lowering thermal conductivity, which focuses on introducing extra scattering points into the structure of the material. Furthermore, enhancing electrical properties entails fine-tuning carrier concentration, opening up a bandgap, and reducing the effective mass of charge carriers [30,34–36]. Numerous studies have endeavored to address the limitations in enhancing the *ZT* of graphene by introducing diverse defects into the hexagonal lattice of graphene.

Recent investigations indicate that substantial heteroatom doping of graphene can enhance its thermoelectric capabilities [37,38]. For example, the phonon scattering rate is not only influenced by deliberately introduced defects but also have the potential to induce a bandgap in graphene. Experimental observations have revealed an increase in *ZT* for graphene through the introduction of defects via high-power irradiation [35], grain boundaries [36], and nanomeshes [39]. Certain theoretical examinations of graphene nanoribbons have shown that disorder along zig-zag edges, nanopore [40], and suitable combinations of vacancies and carbon isotopes [41] have the potential to greatly increase thermoelectric conversion efficiency. This is achieved by effectively reducing thermal conductivity and its impact on electrical properties. Insight into the impact of defects on graphene as an energy management material is necessary to achieve the targeted engineering goals [33].

Alternatively, graphene presents an attractive option due to its inherent flexibility and high electrical conductivity. Several theoretical investigations have proposed the outstanding thermoelectric capability of the graphene structure [42,43]. Experimental findings have also indicated remarkably high power factors in both films grown through chemical vapor deposition (CVD) [44,45] and isolated graphene flakes [23]. Doping graphene has garnered significant attention, as it is crucial in manufacturing integrated devices. Lately, considerable interest has focused on clusters and adatoms of metal on graphene due to their capacity to selectively dope or alter the band structure at a local level [46,47]. An understanding of how electrons, metals, and molecules interact with graphene is essential to achieve effective doping and high electronic mobility for various applications. It is also possible for metal adatoms to significantly change the structure of graphene. The absorption of metal nanoparticles leads to shifts in both the structural and electronic characteristics of graphene. Therefore, understanding their structural impact and electronic characteristics of graphene holds significance. However, the physics governing the interface between metallic electrodes and graphene remains uncertain. Investigations into altering graphene defects with other metal adatoms have been conducted. Currently, no literature studies the thermoelectric properties of Au deposited on graphene. As determined using DFT, the electronic structure and charge transfer of the graphene/metal interface revealed the physisorption of graphene onto surfaces such as Pt, Ag, Al, Au, and Cu. Interestingly, Au is highly resistant to oxidation and corrosion, making it suitable for use in various environments without significant degradation over time. Furthermore, since the work function of graphene is lower than that of Au metal (the work function of Au is 5.47 eV and the work function of graphene is around 4.5–4.6 eV), the formed ohmic junction can thus tune carrier concentration [48,49]. Nevertheless, experimental investigations of metal/graphene systems are still limited, and it remains crucial to comprehend their impact on the structural and electronic properties of graphene. It is essential to study the impact of metal doping on the structure of graphene and its potential for altering chemical and thermoelectric properties. Nevertheless, limited research has focused on investigating the structural characterization and thermoelectric properties of metal-doped graphene, especially in the case of Au.

In this study, we examined the thermoelectric characteristics of multilayer graphene films by introducing deposited Au atoms. We present findings regarding the influence of a thin Au deposited on multilayer graphene grown using CVD, employing techniques such as Raman spectroscopy, SEM-EDX, and thermoelectric measurements. The outcomes from both Raman spectra and transport assessments reveal that Au affects both the structural and electronic properties of graphene. We conducted analyses on Raman bands before and after Au deposition with varying thicknesses of 7 nm and 10 nm on multilayer graphene. In addition, we also include calculations using DFT to study the thermoelectric properties of Au-doped graphene. Furthermore, thermoelectric measurements of Au-deposited graphene multilayer samples showed a p-type doping effect. The optimization methods employed in this study hold the potential to pave a promising path toward improving the thermoelectric properties of graphene materials.

## 2. Experimental details

### 2.1. Sample preparation

Multilayer CVD graphene (2 in × 2 in) on single-sided copper (Cu) foil with a thickness of 35 μm was purchased from the ACS Materials, LLC (www.acsmaterial.com). First, we cut the original size of multilayer graphene (MLG) film into smaller pieces (2 cm × 0.5 cm). Next, we deposited Au on top of graphene film using a LUXOR Au – SEM Coater at a setpoint of 7 and 10 nm thickness, labeled as MLG-Au1 and MLG-Au2, respectively. A schematic illustration of MLG films on Cu substrate is presented in Fig. 1(a).

### 2.2. Characterization

The characterization of MLG film samples was carried out using a Raman spectrometer, operating at a laser excitation wavelength of 532 nm. The morphology and chemical compositions analysis (quantitative analysis of constituent elements) of samples were performed using SEM-EDX (JEOL JSM-6510LA) at energy range of 0–20 keV, a voltage of 15

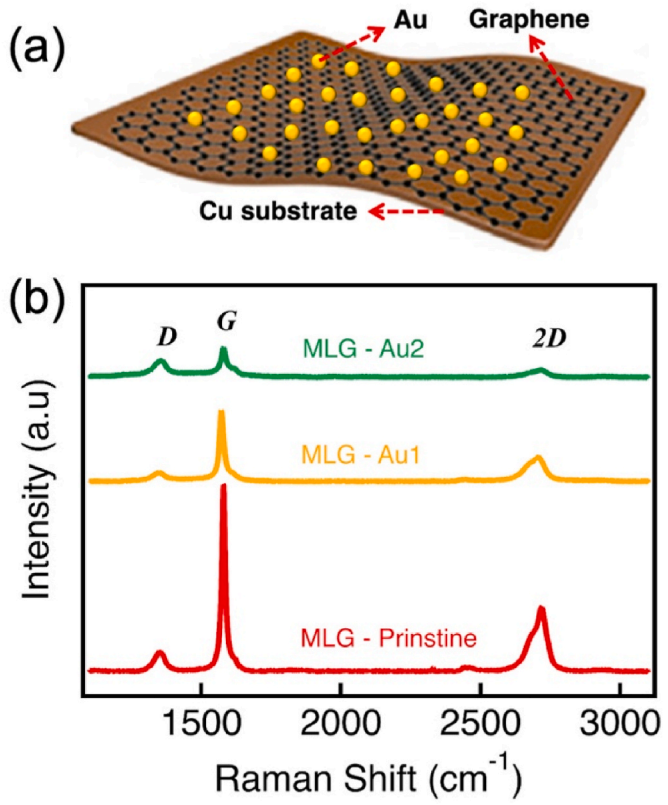


**Fig. 1.** (a) Schematic illustration and (b) The Raman spectra of the MLG-Pristine and after Au deposition MLG-Au1 and MLG-Au2.

kV, and pixel resolution of 1024 × 768. The probe current emitted electrons and determined secondary or backscattered electrons with an emission of 1 nA. LSR-4 instrument (Linseis, Germany) was employed to quantify the thermoelectric properties of MLG film samples at a low pressure of 0.2 bar in a helium atmosphere. The temperature range for measurements was 332 K–552 K, with a temperature interval of 1.8 K. The four-point probe method is used to measure electrical resistivity with an applied current of 100 mA and a distance of 0.6 cm between voltage probes. According to the previous research, the Seebeck voltage is divided by the Ohmic voltage [50]. The sample was measured for its thermoelectricity in a free-standing position.

### 2.3. Computational section

Calculations of the thermoelectric properties of Au-doped gaphene were carried out using first principles calculations and semi-classical Boltzmann theory. The initial calculations carried out were optimization of the geometry and electronic structure of Au-doped graphene using DFT [51,52] with OpenMX code [53]. Thermoelectric properties are calculated using BoltzTraP software based on semi-classical Boltzmann theory through physical quantities and depending on the chemical potential μ [54–56].

## 3. Results and discussion

### 3.1. Structural characterization

The Raman spectra of MLG films on Cu for pristine (MLG-Pristine) and after Au-deposited samples (MLG-Au1 and MLG-Au2) are shown in Fig. 1(b). The intensity, peak position, and shape are important indicators of the graphene structure and number of layers [57]. The presence of graphene's disorder is revealed by the presence of D-band (disorder mode) associated with the out-of-plane breathing mode of sp2 atoms. The G-band corresponds to the $sp^2$ C═C stretching vibrations and $E_{2G}$ phonon in the central Brillouin zone. Inspecting the quality of graphene is done using the 2D-band [58–60]. The D, G, and 2D peaks of MLG-Pristine are observed at 1346, 1576, and 2700 $cm^{-1}$, respectively. Compared to MLG-Pristine, the D, G, and 2D modes of the MLG-Au1 sample are attributed to the peaks at 1349, 1572, and 2707 $cm^{-1}$, respectively. The D, G, and 2D peaks of the MLG-Au2 sample are located at 1358, 1580, and 2713 $cm^{-1}$, respectively. The MLG-Pristine sample has a 2D peak, which is around 2700 $cm^{-1}$, which shifts to around 2707 $cm^{-1}$ for MLG-Au1 and around 2713 $cm^{-1}$ for MLG-Au2. All the Raman spectra of samples are consistent with earlier works [57]. Depending on defects, the two fold resonance Raman processes occurring in both intra and inter-valleys activate the D and G peaks to provide the vanishing momentum required to complete the resonant mode [57,61]. Therefore, the increasing in the D and G peaks is influenced by the increasing in defect concentration.

The first-order Raman band (G band) reveals features related to stretching in the plane of the C–C bond. The G-band exhibits characteristics in nanostructured systems due to the effect of quantum confinement, curvature effects, and electron-phonon coupling. The strong C–C bond and the small mass of the C atom lead to a relatively high G band Raman frequency in $sp^2$ carbon materials [62]. The G peak shifted from 1576 $cm^{-1}$ to 1572 $cm^{-1}$ (MLG-Au1) and 1580 $cm^{-1}$ (MLG-Au2) after Au deposition, indicating that metal (Au) deposition induces doping in graphene [61]. Fig. 1(b) also illustrates that the deposition of Au onto graphene can serve as a dopant, introducing additional charge carriers into the graphene channel and increasing the concentration of impurity carriers [63]. The 2D band is sensitive to minor charges in the electronic structure and vibrational structure, serving as a probe for electrons and phonons, with unique characteristics in each $sp^2$ nanocarbon [62]. The changes in the intensity of the D, G, and 2D peaks were observed after 7 nm and 10 nm Au deposition, as shown in Fig. 1(b). The $I_{2D}/I_G$ and $I_D/I_G$ ratio for MLG-Pristine and after Au deposition are presented in Table 1, indicating defects in graphene. For the MLG-pristine, the $I_D/I_G$ ratio is 0.19 and the $I_{2D}/I_G$ ratio is 0.37.

The D band is generated by additional charges, ripples, and disruption in the atomic arrangement of the material [64]. The D band has also been associated with boundaries and interfaces. The $I_D/I_G$ ratio is inversely proportional to the size of crystallite $L_a$ according to equation (1) [62].

$$I_D \Big/ I_G = \frac{A}{L_a} \tag{1}$$

where $A$ is the fixed Raman excitation frequency constant. The ratio of $I_D/I_G$ decreased in the MLG-Pristine from 0.19 to 0.13 after the deposition of 7 nm of Au (MLG-Au1). However, the MLG-Au2 sample exhibited a much higher $I_D/I_G$ ratio than MLG-Pristine, indicating a strong D peak in the MLG-Au2 sample compared to MLG-Pristine. The significantly increased $I_D/I_G$ ratio in MLG-Au2 (from 0.19 to 0.56) compared to MLG-Pristine suggests a higher density of structural defects in the MLG-Au2 sample and the growth of fine crystalline phase [65,66]. This can be attributed to (i) the presence of amorphous phase growth; and (ii) the destruction and multiplication of crystallites [66]. The higher $I_D/I_G$ ratio indicates a greater presence of structural defects in the MLG-Au2 sample compared to the MLG-Pristine sample [62,65]. The increasing the $I_D/I_G$ ratio confirms the formation of a more disordered structure obtained by increasing the doping of the sample, the D band increases along with the

**Table 1**
The $I_D/I_G$ and $I_{2D}/I_G$ ratio of the MLG-Pristine and after Au deposition.

| Sample | $I_{2D}/I_G$ | $I_D/I_G$ |
|---|---|---|
| MLG – Pristine | 0.37 | 0.19 |
| MLG - Au1 | 0.34 | 0.13 |
| MLG - Au2 | 0.25 | 0.56 |

decrease and broadening of the 2D band [67]. The presence of defects increases the $I_D/I_G$ value [68]. Symmetry breaking occurs due to the presence of interstitial atoms, vacancies, and substitution atoms [69]. The symmetry-breaking that leads to the disorder-induced D band can provide important insights into localized disorder. The D band corresponds to a secondary mechanism involving inelastic scattering [62]. These disorder induced by inelastic scattering may alter the thermal and electrical conductivity, hence the Seebeck coefficient in thermoelectric properties.

The $I_{2D}/I_G$ ratio for MLG-Au1 becomes 0.34 compared to 0.37 for MLG-Pristine. The $I_{2D}/I_G$ ratio also decreased to 0.25 for MLG-Au2. MLG-Au1 indicates a lower $I_D/I_G$ values compared to pure MLG. This is possibly due to the size of the MLG-Au1 crystallites is slightly larger than the size of the MLG-pristine crystallites. As a result, an increase in the number of defects at grain boundaries causing the $I_D/I_G$ value of MLG-Au1 to be slightly lower than MLG-pristine. Likewise with $I_D/I_G$ MLG-Au2 is also bigger than the others sample because the crystal size is small. All the observed changes in the Raman spectrum are primarily attributed to the introduced Au deposition and the increased rate of photoexcited scattering of electrons with those defects [64,70]. The differences in the $I_{2D}/I_G$ ratio and the positions of the 2D peak, G peak, and D peak demonstrate variations among samples with differing quantities of graphene layers [66].

Figs. 2–4 depict the typical morphology and elemental composition of MLG-Pristine and samples after Au deposition samples via SEM-EDX. SEM image of the MLG-Pristine surface is shown at the magnification of 1000 × (Fig. 2(a)). The image of pristine graphene (MLG-Pristine) displays a relatively uniform appearance, illustrating the exceptional quality of the MLG-Pristine with minor residue, characterized by enhanced brightness in the region with wrinkles [26,71]. In Fig. 2(b)–a quantitative analysis of MLG-Pristine is presented, with the EDX spectrum showing the C and Cu peaks. The concentration of C atoms is estimated to be 51.21%, and Cu is 48.79%, distributed throughout the sample area. Confirmation of the presence of C and Cu elements can be observed in the element distribution on the MLG-Pristine surface (Fig. 2 (d–f)).

Fig. 3 presents SEM and EDX elemental mapping images of MLG-Au1. The SEM image of the MLG-Au1 sample reveals the distribution of Au on the graphene surface. Fig. 3(a) shows the largest Au diameter is 0.67 μm, with Au distributed sparsely and evenly on the surface of the sample. A quantitative analysis of the MLG-Au1 sample, with the EDX spectrum displaying C, Au, and Cu peaks (Fig. 3(b)). The concentration of C atoms is estimated to be 33.23%, the Au is 2.19%, and the Cu is 64.58%, spread throughout the sample area. Confirmation of the presence of C, Au, and Cu elements can be observed in the element distribution on the MLG-Au1 surface according to Fig. 3(c–f).

Fig. 4(a) depicts the distribution of Au on the MLG-Au2 sample. The SEM image reveals the presence of small bright spots, indicating the presence of Au, with an increased amount compared to the MLG-Au1 sample. The size distribution of the MLG-Au2 sample shows that the maximum Au diameter size is 1 μm. The distribution of Au was found to be denser on the sample surface compared to the MLG-Au1 sample. This is consistent with the Au deposits formed during the doping process, which spread across the surface in line with the increased Au concentration [71]. Fig. 4(b) presents a quantitative analysis of MLG-Au2, with the EDX spectrum displaying C, Au, and Cu peaks. The concentration of C atoms is estimated to be 39.54%, the Au is 3.98%, and the Cu is 56.48%, distributed throughout the sample area. Confirmation of the presence of C, Au, and Cu elements can be observed in the element distribution on the MLG-Au2 surface (Fig. 4(c–f)).

### 3.2. Thermoelectric properties

The fundamental mechanism responsible for the increase in thermoelectric properties is analyzed through the Seebeck coefficient, resistivity, and power factor [66]. The thermoelectric properties of the MLG-Pristine and MLG-Au were measured in the temperature range of 332 K–552 K. The temperature dependence of the Seebeck coefficient ($S$) for MLG-Pristine and Au deposited samples is represented in Fig. 5(a). The Seebeck coefficient values of MLG-Pristine, MLG-Au1, and MLG-Au2 are proportional to the increase in temperature, as described by the following equation (2) [72,73].

$$S = \frac{8\pi^2 k_B^2}{3eh^2} m^* T \left(\frac{\pi}{3n}\right)^{\frac{2}{3}} (1+R) \tag{2}$$

where $m^*$ is the effective mass of the charge carriers, $k_B$ is the Boltz-

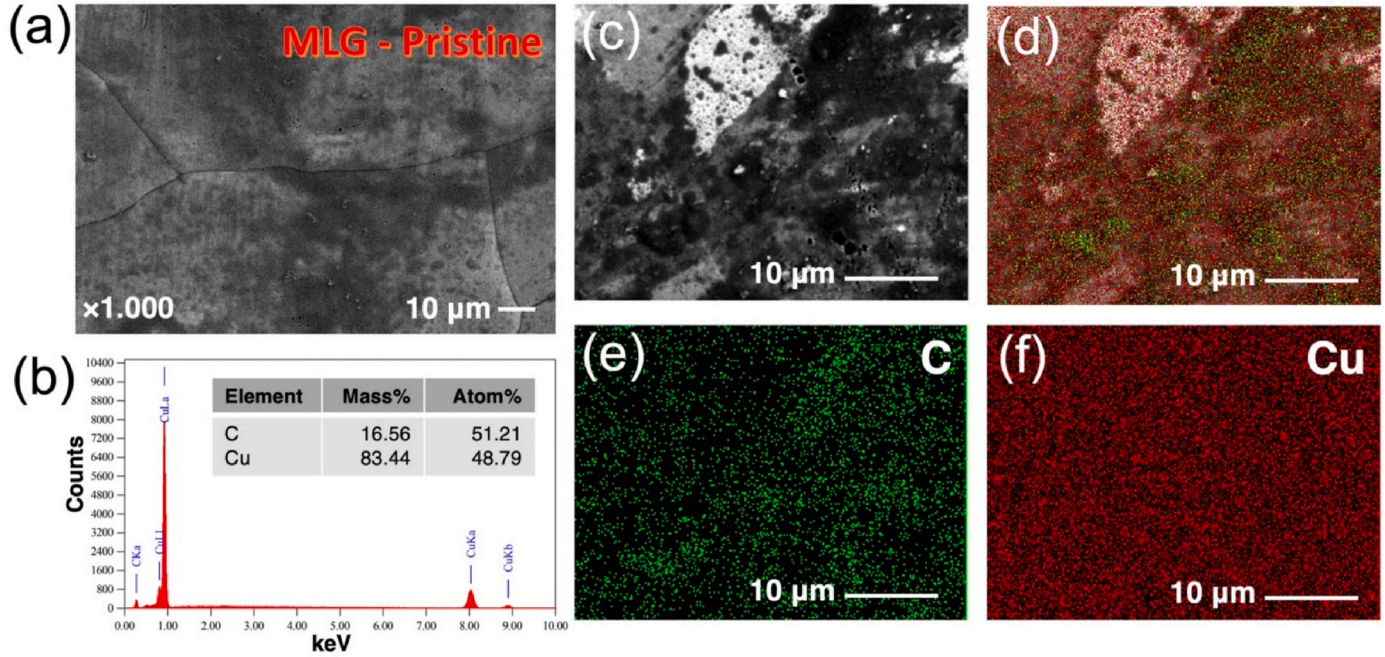


**Fig. 2.** SEM and EDX elemental mapping images of MLG-Pristine: (a and c) morphology, (b) EDX spectra (insert table for the atomic and mass percentage of various elements), (d) total, (e) C, and (f) Cu.

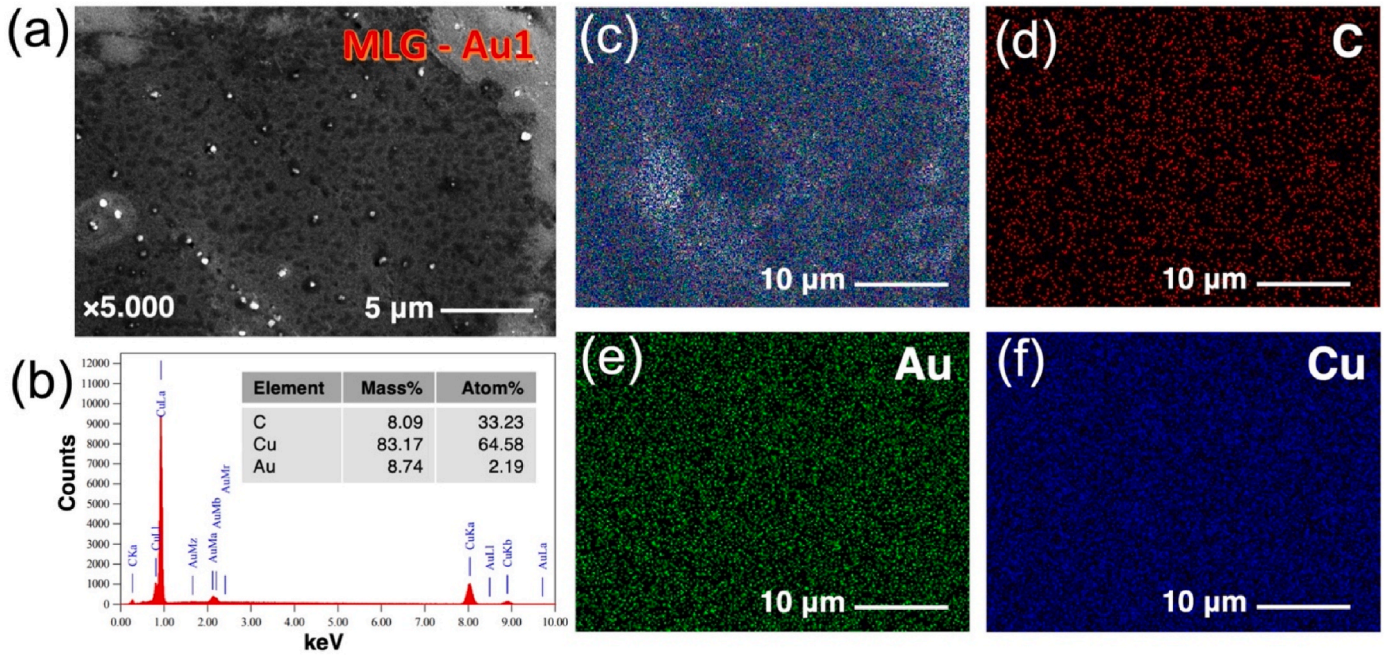


**Fig. 3.** SEM and EDX elemental mapping images of MLG-Au1: (a) morphology, (b) EDX spectra (insert table for the atomic and mass percentage of various elements), (c) total, (d) C, (e) Au, and (f) Cu.

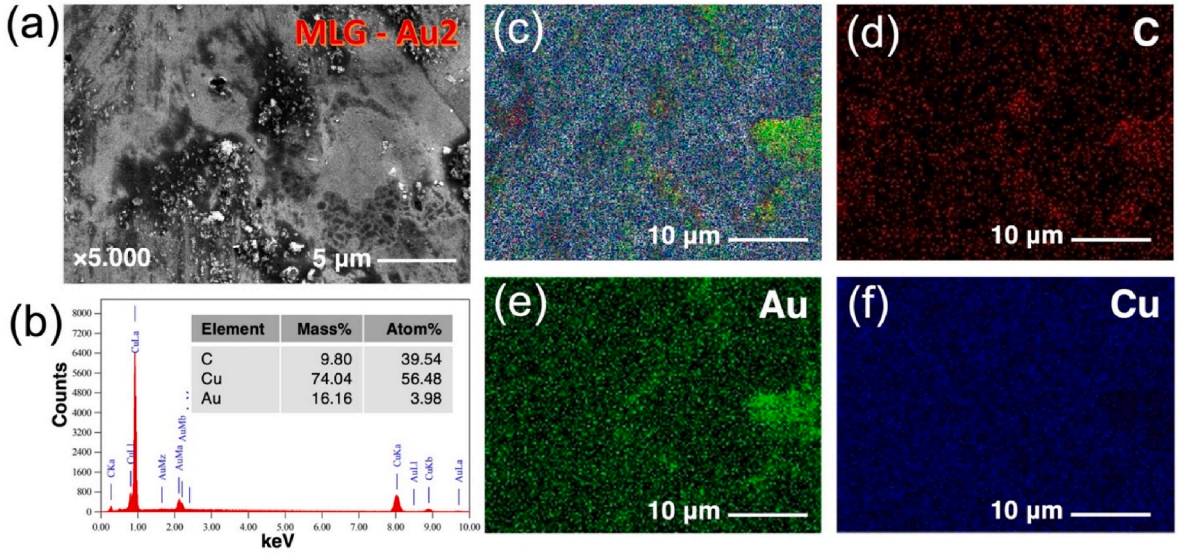


**Fig. 4.** SEM and EDX elemental mapping images of MLG-Au2: (a) morphology, (b) EDX spectra (insert table for the atomic and mass percentage of various elements), (c) total, (d) C, (e) Au, and (f) Cu.

mann's constant, $T$ is the absolute temperature, $h$ is the Planck's constant, $n$ is the concentration of carrier and $R$ is the scattering function. The Seebeck coefficient value of MLG-Au1 at 332 K is 1.2 μV/K, and for MLG-Au2 is 1.67 μV/K. This represents an increase compared to the Seebeck coefficient value of MLG-Pristine, which is 0.53 μV/K. It demonstrates that doping increases the Seebeck coefficient across the entire temperature range. The maximum Seebeck coefficient of the MLG-Au1 within the measured temperature range reaches 3.17 μV/K at 528 K, compared to 0.66 μV/K at 552 K for MLG-Pristine (Fig. 5(a)). With further increases in the Au deposition treatment, we observe that the maximum Seebeck coefficient of MLG-Au2 can be increased to 4.67 μV/K at 528 K, in contrast to 0.66 μV/K at 552 K for MLG-Pristine. Comparison with the Seebeck coefficient value of graphene reported in the previous literature [1] revealed that the experimental results still exhibited relatively low values. This can be attributed to the substrate's influence used during the thermopower measurement. The substrate employed for thermoelectric measurements is Cu, known for its excellent conductivity.

The Cu substrate significantly contributes to the Seebeck coefficient of the measured MLG samples, resulting in only a slight increase in the Seebeck coefficient of MLG-Au compared to MLG-Pristine. The Seebeck coefficient value of Cu at a temperature of 273 K is 1.70 μV/K [74]. Fig. 5 (a) illustrates that the Seebeck coefficient ($S$) for all samples exhibit positive signs and demonstrate an increasing trend with temperature [66]. Consequently, it is evident that MLG-Pristine, MLG-Au1, and MLG-Au2 show p-type conduction due to the introduction of deposited Au [75]. Since both hole and electron mobility contribute to the sign of the Seebeck coefficient [26], the p-type characteristic

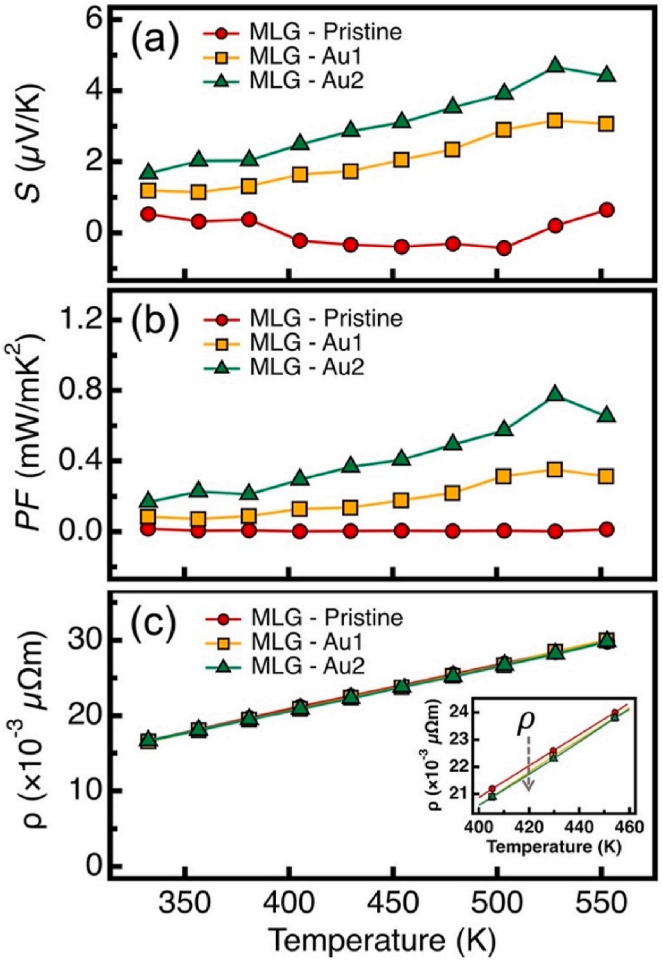


**Fig. 5.** The dependence on temperature of the MLG-Pristine and after Au deposition (MLG-Au1 and MLG-Au2): (a) Seebeck coefficient, (b) power factor, and (c) resistivity.

observed in pristine and Au-deposited graphene indicates that, across the entire temperature range, hole mobility exceeds that of electrons. This implies that holes are the dominant carriers [66]. This behavior arises because, at these temperature ranges, Au acts as an acceptor dopant in the investigated MLG, initiating an intrinsic carrier contribution [76]. Change transfer doping is achieved by exchanging electrons with graphene, involving electron transfer either from dopants to graphene (resulting in n-type graphene) or from graphene to dopants (p-type graphene) [77].

The numerator of the equation $S^2\sigma$ represented the power factor (*PF*) can be used to assess the thermoelectric capabilities of the materials when the thermal conductivity of a material is unknown [78]. Therefore, increasing the *PF* and reducing the thermal conductivity are crucial for raising the *ZT* value [75,79]. In this study, at the temperature of 332 K, the *PF* value of the MLG-Pristine is 0.017 mW/mK$^2$, MLG-Au1 is 0.09 mW/mK$^2$, MLG-Au2 is 0.17 mW/mK$^2$. This demonstrates that the increasing doping enhances the *PF* across the entire temperature range. After 7 nm Au deposition, the maximum *PF* of the MLG within the measured temperature range increases to 0.35 mW/mK$^2$ at 528 K, compared to 0.014 mW/mK$^2$ at 552 K for MLG-Pristine. As the deposition treatment is increased further to 10 nm, we observe that the maximum *PF* can be increased to 0.77 mW/mK$^2$ at 528 K, compared to 0.014 mW/mK$^2$ at 552 K for MLG-Pristine. We found that there was an increase in maximum *PF* to 0.77 mW/mK$^2$ at 528 K, compared to 0.014 mW/mK$^2$ at 552 K for MLG-Pristine in the deposition treatment to 10 nm. An increase in $I_D/I_G$ from 0.13 (MLG-Au1) to 0.56 (MLG-Au2) associates with improvement in the *PF* value by 11 times (MLG-Au1) to 24 times (MLG-Au2) compared to MLG-Pristine. Thus, the significant enhancement in the thermopower of MLG samples after Au deposition is influenced by the formation of structural disorders/defects. Consequently, the increase in the thermopower of MLG samples after Au deposition is directly related to the increase in the formation of structural defects/disorders [26].

The average resistivity values of MLG are $23.3 \times 10^{-9}$ Ωm for MLG-Pristine, $23.18 \times 10^{-9}$ Ωm for MLG-Au1, and $23.12 \times 10^{-9}$ Ωm for MLG-Au2 was measured by a four-point probe using LSR-4 at temperatures of 330 K–550 K. The thermoelectric findings and Raman spectra suggest that the MLG samples with greater structural defects exhibit higher thermopower than the MLG-Pristine. Consequently, there is a desire to deliberately induce additional structural imperfections in the samples to explore their thermoelectric characteristics further. A comparison of thermoelectric properties of our results with the recently published articles in this field presented in Table 2.

In accordance with the experimental results, the calculation results also show that the addition of Au will slightly increase the thermoelectric properties. Fig. 6 shows that the addition of Au (6.25% Au doped graphene) can increase the thermoelectric properties indicated by the maximum value of the seebeck coefficient of 464 $\mu V/K$ (for pristine graphene) become 474 $\mu V/K$ (for 6.25%Au-doped graphene) at $T = 300\ K$ due to the a localized state at energy levels of $\sim -1.3$ eV. It is formed from the existence of the *d* orbital of Au. The Fermi level shifting (about 0.41 eV for 6.25% Au-doped graphene) is due to the transfer of charge from the graphene to the Au atoms indicating that Au-doped graphene is the p-type character of charge carrier (electron-deficient).

## 4. Conclusions

In summary, we study the impact of Au deposition on multilayer graphene using Raman spectroscopy, SEM-EDX, and thermoelectric measurement in a temperature range of 332 K–552 K. The maximum Seebeck coefficient obtained was around 4.67 μV/K at 528 K, significantly improving compared to the 0.66 μV/K and there was an increasing in power factor by 24 times compared to pristine graphene. All samples showed p-type conduction as indicated by positive Seebeck coefficient values where the dominant charge carriers are holes. This study presents a straightforward and efficient approach to enhance the thermoelectric properties of graphene, a promising material with substantial thermoelectric potential.

## CRediT authorship contribution statement

**Dwi Nugraheni Rositawati:** Conceptualization, Data curation, Formal analysis, Investigation, Methodology, Writing – original draft, Writing – review & editing. **Eri Widianto:** Validation, Visualization, Writing – original draft, Writing – review & editing. **Suprapto:** Investigation, Methodology, Investigation, Methodology. **Tjipto Sujitno:** Investigation, Methodology. **Moh. Adhib Ulil Absor:** Methodology, Software, Validation. **Sholihun:** Methodology, Validation, Methodology, Validation. **Kuwat Triyana:** Supervision, Validation. **Iman Santoso:** Project administration, Supervision, Validation, Writing – review & editing.

**Table 2**
Thermoelectric properties of graphene.

| Material | *S* ($\mu V/K$) | *PF* ($\mu W/mK^2$) | Ref. |
|---|---|---|---|
| Multilayer graphene | – | 6000 | [80] |
| $Al_2O_3$/SLG/$HfO_2$ | 70 | – | [81] |
| centimeter-scale monolayer graphene | 350 | 14000 | [82] |
| $Ag_2Se$/rGO nanocomposites | – | 923 | [83] |
| $Bi_2S_3$/GO | 321 | 100 | [84] |
| PbSe-graphene nanocomposite | 2000 | 1300 | [85] |
| Au doped multilayer graphene | 4.67 | 770 | This work |

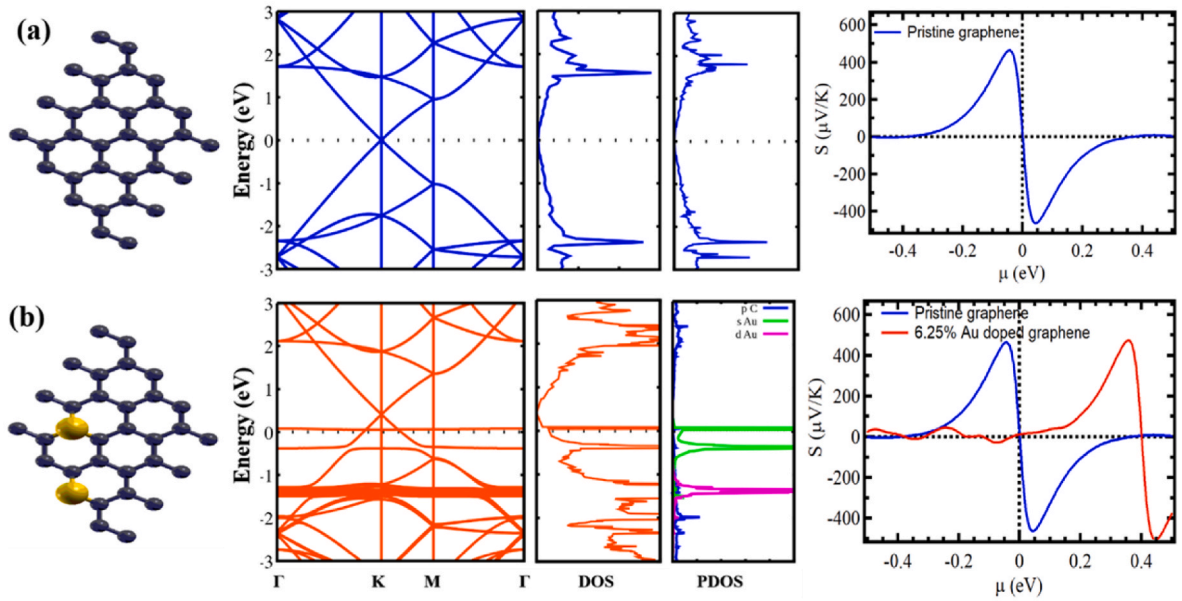


**Fig. 6.** Structure, band structure, DOS, PDOS, and calculated Seebeck coefficient (S) vs chemical potential ($\mu$) for (a) pristine graphene, (b) 6.25% Au-doped graphene. The gold and black spheres show Au and carbon atoms, respectively. (For interpretation of the references to colour in this figure legend, the reader is referred to the Web version of this article.)

## Declaration of competing interest

The authors declare that they have no known competing financial interests or personal relationships that could have appeared to influence the work reported in this paper.

## Data availability

Data will be made available on request.

## Acknowledgments

We would like to thanks Dedi and Mohammad Dani Al qori from research centre for electronic BRIN Indonesia for thermoelectric measurement as well as Virginia Fahriza Amaliya from Integrated Laboratorium for Research and Testing (LPPT) Universitas Gadjah Mada for assisting the SEM measurement. This work was supported by "Kemdikbud – Indonesia" through the "Beasiswa Pendidikan Pascasarjana Dalam Negeri (BPPDN)" 2019 scholarship program.

## References

[1] R. Mulla, A.O. White, C.W. Dunnill, A.R. Barron, The role of graphene in new thermoelectric materials, Energy Adv. (2023), https://doi.org/10.1039/d3ya00085k.
[2] R. Ovik Fitriani, B.D. Long, M.C. Barma, M. Riaz, M.F.M. Sabri, S.M. Said, R. Saidur, A review on nanostructures of high-temperature thermoelectric materials for waste heat recovery, Renew. Sustain. Energy Rev. 64 (2016) 635–659, https://doi.org/10.1016/j.rser.2016.06.035.
[3] D. Beretta, N. Neophytou, J.M. Hodges, M.G. Kanatzidis, D. Narducci, M. Martin-Gonzalez, M. Beekman, B. Balke, G. Cerretti, W. Tremel, A. Zevalkink, A. I. Hofmann, C. Müller, B. Dörling, M. Campoy-Quiles, M. Caironi, Thermoelectrics: from history, a window to the future, Mater. Sci. Eng. R Rep. 138 (2019), https://doi.org/10.1016/j.mser.2018.09.001.
[4] C. Gayner, K.K. Kar, Recent advances in thermoelectric materials, Prog. Mater. Sci. 83 (2016) 330–382, https://doi.org/10.1016/j.pmatsci.2016.07.002.
[5] J. He, T.M. Tritt, Advances in thermoelectric materials research: looking back and moving forward, Science (1979) (2017) 357, https://doi.org/10.1126/science.aak9997.
[6] Y.X. Chen, X.L. Shi, Z.H. Zheng, F. Li, W. Di Liu, W.Y. Chen, X.R. Li, G.X. Liang, J. T. Luo, P. Fan, Z.G. Chen, Two-dimensional $WSe_2$/SnSe p-n junctions secure ultrahigh thermoelectric performance in n-type Pb/I Co-doped polycrystalline SnSe, Materials Today Physics 16 (2021), https://doi.org/10.1016/j.mtphys.2020.100306.
[7] W.Y. Chen, X.L. Shi, J. Zou, Z.G. Chen, Thermoelectric coolers for on-chip thermal management: materials, design, and optimization, Mater. Sci. Eng. R Rep. 151 (2022), https://doi.org/10.1016/j.mser.2022.100700.
[8] A. Pal, K. Shyam Prasad, K. Gurukrishna, S. Mangavati, P. Poornesh, A. Rao, Y. C. Chung, Y.K. Kuo, Enhancement of low-temperature thermoelectric performance via Pb doping in Cu3SbSe4, J. Phys. Chem. Solid. 175 (2023), https://doi.org/10.1016/j.jpcs.2022.111197.
[9] R. Mulla, C.W. Dunnill, Core-shell nanostructures for better thermoelectrics, Mater Adv 3 (2022) 125–141, https://doi.org/10.1039/d1ma00955a.
[10] T. Cao, X.L. Shi, Z.G. Chen, Advances in the design and assembly of flexible thermoelectric device, Prog. Mater. Sci. 131 (2023), https://doi.org/10.1016/j.pmatsci.2022.101003.
[11] N. Xin, G. Tang, T. Lan, Y. Li, J. Kou, M. Zhang, X. Zhao, Y. Nie, Improving the thermoelectric performance of Cu-doped $MoS_2$ film by band structure modification and microstructural regulation, Appl. Surf. Sci. 611 (2023), https://doi.org/10.1016/j.apsusc.2022.155611.
[12] T. Taniguchi, T. Ishibe, N. Naruse, Y. Mera, M.M. Alam, K. Sawano, Y. Nakamura, High thermoelectric power factor realization in Si-rich SiGe/Si superlattices by super-controlled interfaces, ACS Appl. Mater. Interfaces 12 (2020) 25428–25434, https://doi.org/10.1021/acsami.0c04982.
[13] L. Su, D. Wang, S. Wang, B. Qin, Y. Wang, Y. Qin, Y. Jin, C. Chang, L.-D. Zhao, High thermoelectric performance realized through manipulating layered phonon-electron decoupling, Science (1979) 375 (2022) 1385–1389, https://doi.org/10.1126/science.abn8997.
[14] T. Terada, Y. Uematsu, T. Ishibe, N. Naruse, K. Sato, T.Q. Nguyen, E. Kobayashi, H. Nakano, Y. Nakamura, Giant enhancement of seebeck coefficient by deformation of silicene buckled structure in calcium-intercalated layered silicene film, Adv. Mater. Interfac. 9 (2022), https://doi.org/10.1002/admi.202101752.
[15] D. Joseph, M. Navaneethan, R. Abinaya, S. Harish, J. Archana, S. Ponnusamy, K. Hara, Y. Hayakawa, Thermoelectric performance of Cu-doped $MoS_2$ layered nanosheets for low grade waste heat recovery, Appl. Surf. Sci. 505 (2020), https://doi.org/10.1016/j.apsusc.2019.144066.
[16] S. Yadav, S. Chaudhary, D.K. Pandya, Incorporation of MoS 2 nanosheets in $CoSb_3$ matrix as an efficient novel strategy to enhance its thermoelectric performance, Appl. Surf. Sci. 435 (2018) 1265–1272, https://doi.org/10.1016/j.apsusc.2017.11.262.
[17] S.S. Lee, I. Jang, J.S. Rhyee, S.J. Hong, S. Jong Yoo, I.K. Park, Enhanced thermoelectric performance of Mo nanoparticle decorated n-type $Bi_2Te_{2.7}Se_{0.3}$ powder composites, Appl. Surf. Sci. 548 (2021), https://doi.org/10.1016/j.apsusc.2021.149200.
[18] A.K. Geim, K.S. Novoselov, The rise of graphene, Nat. Mater. 6 (2007) 183–191, https://doi.org/10.1038/nmat1849.
[19] A.H. Castro Neto, F. Guinea, N.M.R. Peres, K.S. Novoselov, A.K. Geim, The electronic properties of graphene, Rev. Mod. Phys. 81 (2009) 109–162, https://doi.org/10.1103/RevModPhys.81.109.
[20] K.S. Novoselov, V.I. Fal'Ko, L. Colombo, P.R. Gellert, M.G. Schwab, K. Kim, A roadmap for graphene, Nature 490 (2012) 192–200, https://doi.org/10.1038/nature11458.
[21] W.K. Chee, H.N. Lim, Z. Zainal, N.M. Huang, I. Harrison, Y. Andou, Flexible graphene-based supercapacitors: a review, J. Phys. Chem. C 120 (2016) 4153–4172, https://doi.org/10.1021/acs.jpcc.5b10187.

[22] E. Singh, H.S. Nalwa, Graphene-based bulk-heterojunction solar cells: a review, J. Nanosci. Nanotechnol. 15 (2015) 6237–6278, https://doi.org/10.1166/jnn.2015.11654.

[23] J. Duan, X. Wang, X. Lai, G. Li, K. Watanabe, T. Taniguchi, M. Zebarjadi, E. Y. Andrei, High thermoelectricpower factor in graphene/hBN devices, Proc. Natl. Acad. Sci. U. S. A. 113 (2016) 14272–14276, https://doi.org/10.1073/pnas.1615913113.

[24] P. an Zong, J. Liang, P. Zhang, C. Wan, Y. Wang, K. Koumoto, Graphene-based thermoelectrics, ACS Appl. Energy Mater. 3 (2020) 2224–2239, https://doi.org/10.1021/acsaem.9b02187.

[25] Y. Guo, J. Mu, C. Hou, H. Wang, Q. Zhang, Y. Li, Flexible and thermostable thermoelectric devices based on large-area and porous all-graphene films, Carbon N Y 107 (2016) 146–153, https://doi.org/10.1016/j.carbon.2016.05.063.

[26] N. Xiao, X. Dong, L. Song, D. Liu, Y. Tay, S. Wu, L.J. Li, Y. Zhao, T. Yu, H. Zhang, W. Huang, H.H. Hng, P.M. Ajayan, Q. Yan, Enhanced thermopower of graphene films with oxygen plasma treatment, ACS Nano 5 (2011) 2749–2755, https://doi.org/10.1021/nn2001849.

[27] A. Yousefzadi Nobakht, S. Shin, K.D. Kihm, D.C. Marable, W. Lee, Heat flow diversion in supported graphene nanomesh, Carbon N Y 123 (2017) 45–53, https://doi.org/10.1016/j.carbon.2017.07.025.

[28] H.G. Kim, K.D. Kihm, W. Lee, G. Lim, S. Cheon, W. Lee, K.R. Pyun, S.H. Ko, S. Shin, Effect of graphene-substrate conformity on the in-plane thermal conductivity of supported graphene, Carbon N Y 125 (2017) 39–48, https://doi.org/10.1016/j.carbon.2017.09.033.

[29] H. Jang, Y.J. Park, X. Chen, T. Das, M.S. Kim, J.H. Ahn, Graphene-based flexible and stretchable electronics, Adv. Mater. 28 (2016) 4184–4202, https://doi.org/10.1002/adma.201504245.

[30] P. Dollfus, V.H. Nguyen, J. Saint-Martin, Thermoelectric effects in graphene nanostructures, J. Phys. Condens. Matter 27 (2015), https://doi.org/10.1088/0953-8984/27/13/133204.

[31] P. an Zong, J. Liang, P. Zhang, C. Wan, Y. Wang, K. Koumoto, Graphene-based thermoelectrics, ACS Appl. Energy Mater. 3 (2020) 2224–2239, https://doi.org/10.1021/acsaem.9b02187.

[32] S.J. Zhang, S.S. Lin, X.Q. Li, X.Y. Liu, H.A. Wu, W.L. Xu, P. Wang, Z.Q. Wu, H. K. Zhong, Z.J. Xu, Opening the band gap of graphene through silicon doping for the improved performance of graphene/GaAs heterojunction solar cells, Nanoscale 8 (2016) 226–232, https://doi.org/10.1039/c5nr06345k.

[33] W. Lee, G. Lim, S.H. Ko, Significant thermoelectric conversion efficiency enhancement of single layer graphene with substitutional silicon dopants, Nano Energy 87 (2021), https://doi.org/10.1016/j.nanoen.2021.106188.

[34] W. Lee, K.D. Kihm, H.G. Kim, W. Lee, S. Cheon, S. Yeom, G. Lim, K.R. Pyun, S. H. Ko, S. Shin, Two orders of magnitude suppression of graphene's thermal conductivity by heavy dopant (Si), Carbon N Y 138 (2018) 98–107, https://doi.org/10.1016/j.carbon.2018.05.064.

[35] Y. Anno, Y. Imakita, K. Takei, S. Akita, T. Arie, Enhancement of graphene thermoelectric performance through defect engineering, 2D Mater. 4 (2017), https://doi.org/10.1088/2053-1583/aa57fc.

[36] G. Lim, K.D. Kihm, H.G. Kim, W. Lee, W. Lee, K.R. Pyun, S. Cheon, P. Lee, J.Y. Min, S.H. Ko, Enhanced thermoelectric conversion efficiency of CVD graphene with reduced grain sizes, Nanomaterials 8 (2018), https://doi.org/10.3390/nano8070557.

[37] E. Rahmati, A. Bafekry, M. Faraji, D. Gogva, C.V. Nguyen, M. Ghergherehchi, Thermoelectric properties of doped graphene nanoribbons: density functional theory calculations and electrical transport, RSC Adv. 12 (2022) 6174–6180, https://doi.org/10.1039/D1RA08303A.

[38] S. Ullah, Q. Shi, J. Zhou, X. Yang, H.Q. Ta, M. Hasan, N.M. Ahmad, L. Fu, A. Bachmatiuk, M.H. Rümmeli, Advances and trends in chemically doped graphene, Adv. Mater. Interfac. 7 (2020) 2000999, https://doi.org/10.1002/admi.202000999.

[39] J. Oh, H. Yoo, J. Choi, J.Y. Kim, D.S. Lee, M.J. Kim, J.C. Lee, W.N. Kim, J. C. Grossman, J.H. Park, S.S. Lee, H. Kim, J.G. Son, Significantly reduced thermal conductivity and enhanced thermoelectric properties of single- and bi-layer graphene nanomeshes with sub-10 nm neck-width, Nano Energy 35 (2017) 26–35, https://doi.org/10.1016/j.nanoen.2017.03.019.

[40] M.S. Hossain, F. Al-Dirini, F.M. Hossain, E. Skafidas, High performance graphene nano-ribbon thermoelectric devices by incorporation and dimensional tuning of nanopores, Sci. Rep. 5 (2015), https://doi.org/10.1038/srep11297.

[41] V.T. Tran, J. Saint-Martin, P. Dollfus, S. Volz, Optimizing the thermoelectric performance of graphene nano-ribbons without degrading the electronic properties, Sci. Rep. 7 (2017), https://doi.org/10.1038/s41598-017-02230-0.

[42] Y. Ouyang, J. Guo, A theoretical study on thermoelectric properties of graphene nanoribbons, Appl. Phys. Lett. 94 (2009), https://doi.org/10.1063/1.3171933.

[43] H. Sevinçli, G. Cuniberti, Enhanced thermoelectric figure of merit in edge-disordered zigzag graphene nanoribbons, Phys Rev B Condens Matter Mater Phys 81 (2010), https://doi.org/10.1103/PhysRevB.81.113401.

[44] K. Kanahashi, M. Ishihara, M. Hasegawa, H. Ohta, T. Takenobu, Giant power factors in p- and n-type large-area graphene films on a flexible plastic substrate, NPJ 2D Mater Appl 3 (2019), https://doi.org/10.1038/s41699-019-0128-0.

[45] T.G. Novak, J. Kim, J. Kim, A.P. Tiwari, H. Shin, J.Y. Song, S. Jeon, Complementary n-type and p-type graphene films for high power factor thermoelectric generators, Adv. Funct. Mater. 30 (2020), https://doi.org/10.1002/adfm.202001760.

[46] M.W. Iqbal, A.K. Singh, M.Z. Iqbal, J. Eom, Raman fingerprint of doping due to metal adsorbates on graphene, J. Phys. Condens. Matter 24 (2012), https://doi.org/10.1088/0953-8984/24/33/335301.

[47] G. Giovannetti, P.A. Khomyakov, G. Brocks, V.M. Karpan, J. Van Den Brink, P. J. Kelly, Doping graphene with metal contacts, Phys. Rev. Lett. 101 (2008), https://doi.org/10.1103/PhysRevLett.101.026803.

[48] P.A. Khomyakov, G. Giovannetti, P.C. Rusu, G. Brocks, J. Van Den Brink, P.J. Kelly, First-principles study of the interaction and charge transfer between graphene and metals, Phys Rev B Condens Matter Mater Phys 79 (2009), https://doi.org/10.1103/PhysRevB.79.195425.

[49] K.T. Chan, J.B. Neaton, M.L. Cohen, First-principles study of metal adatom adsorption on graphene, Phys Rev B Condens Matter Mater Phys 77 (2008), https://doi.org/10.1103/PhysRevB.77.235430.

[50] M.D. Al Qori, N.L. Kartika, A.R. Nugraha, B.S. Bhakti, A.R. Mubarok, A. Rusmana, A. Septiani, Dedi, the effect of Ti doping on the thermoelectric performance of $Bi_2Te_3$ and its chemical stability, J. Mater. Eng. Perform. (2023), https://doi.org/10.1007/s11665-023-08444-w.

[51] W. Kohn, L.J. Sham, Self-consistent equations including exchange and correlation effects, Phys. Rev. 140 (1965) A1133–A1138, https://doi.org/10.1103/PhysRev.140.A1133.

[52] P. Hohenberg, W. Kohn, Inhomogeneous electron gas, Phys. Rev. 136 (1964) 3B, https://doi.org/10.1103/PhysRev.136.B864.

[53] T. Ozaki, H. Kino, J. Yu, M.J. Han, M. Ohfuchi, F. Ishii, K. Sawada, Y. Kubota, Y. P. Mizuta, H. Kotaka, N. Yamaguchi, H. Sawahata, T.B. Prayitno, T. Ohwaki, T.V. T. Duy, M. Miyata, G. Jiang, P.H. Chang, A. Terasawa, Y. Gohda, H. Weng, Y. Shiihara, M. Toyoda, Y. Okuno, R. Perez, P.P. Bell, M. Ellner, Y. Xiao, A.M. Ito, M. Otani, M. Kawamura, K. Yoshimi, C.C. Lee, Y.T. Lee, M. Fukuda, S. Ryee, K. Terakura, User's Manual of OpenMX Ver, 3.9, 2020 (Tokyo).

[54] T. Ozaki, Variationally optimized atomic orbitals for large-scale electronic structures, Phys. Rev. B 67 (2003) 155108, https://doi.org/10.1103/PhysRevB.67.155108.

[55] G.K.H. Madsen, D.J. Singh, BoltzTraP. A code for calculating band-structure dependent quantities, Comput. Phys. Commun. 175 (2006) 67–71, https://doi.org/10.1016/j.cpc.2006.03.007.

[56] M. Miyata, T. Ozaki, T. Takeuchi, S. Nishino, M. Inukai, M. Koyano, High-throughput screening of sulfide thermoelectric materials using electron transport calculations with OpenMX and BoltzTraP, J. Electron. Mater. 47 (2018) 3254–3259, https://doi.org/10.1007/s11664-017-6020-9.

[57] A.C. Ferrari, J.C. Meyer, V. Scardaci, C. Casiraghi, M. Lazzeri, F. Mauri, S. Piscanec, D. Jiang, K.S. Novoselov, S. Roth, A.K. Geim, Raman spectrum of graphene and graphene layers, Phys. Rev. Lett. 97 (2006), https://doi.org/10.1103/PhysRevLett.97.187401.

[58] A.C. Ferrari, D.M. Basko, Raman spectroscopy as a versatile tool for studying the properties of graphene, Nat. Nanotechnol. 8 (2013) 235–246, https://doi.org/10.1038/nnano.2013.46.

[59] G. Savini, A.C. Ferrari, F. Giustino, First-principles prediction of doped graphane as a high-temperature electron-phonon superconductor, Phys. Rev. Lett. 105 (2010), https://doi.org/10.1103/PhysRevLett.105.037002.

[60] A.C. Ferrari, S.E. Rodil, J. Robertson, S.E. Rodil, J. Robertson, Interpretation of infrared and Raman spectra of amorphous carbon nitrides, Phys Rev B Condens Matter Mater Phys 67 (2003) 155306, https://doi.org/10.1103/PhysRevB.67.155306.

[61] A.C. Ferrari, D.M. Basko, Raman spectroscopy as a versatile tool for studying the properties of graphene, Nat. Nanotechnol. 8 (2013) 235–246, https://doi.org/10.1038/nnano.2013.46.

[62] A. Jorio, R. Saito, G. Dresselhaus, M.S. Dresselhaus, Raman Spectroscopy in Graphene Related Systems, WILEY-VCH Verlag GmbH & Co. Germany, 2011.

[63] C.A. Joiner, T. Roy, Z.R. Hesabi, B. Chakrabarti, E.M. Vogel, Cleaning graphene with a titanium sacrificial layer, Appl. Phys. Lett. 104 (2014), https://doi.org/10.1063/1.4881886.

[64] Y. Zeng, Y. Zhao, Y. Jiang, Investigate the interface structure and growth mechanism of high quality ZnO films grown on multilayer graphene layers, in: Appl Surf Sci, Elsevier B.V., 2014, pp. 391–395, https://doi.org/10.1016/j.apsusc.2014.02.088.

[65] L. Miao, Y. Jiang, S. Lu, B. Shi, C. Zhao, H. Zhang, S. Wen, Broadband ultrafast nonlinear optical response of few-layers graphene: toward the mid-infrared regime, Photon. Res. 3 (2015) 214, https://doi.org/10.1364/prj.3.000214.

[66] W. Ma, Y. Liu, S. Yan, T. Miao, S. Shi, Z. Xu, X. Zhang, C. Gao, Chemically doped macroscopic graphene fibers with significantly enhanced thermoelectric properties, Nano Res. 11 (2018) 741–750, https://doi.org/10.1007/s12274-017-1683-3.

[67] C.R.S.V. Boas, B. Focassio, E. Marinho, D.G. Larrude, M.C. Salvadori, C.R. Leão, D. J. dos Santos, Characterization of nitrogen doped graphene bilayers synthesized by fast, low temperature microwave plasma-enhanced chemical vapour deposition, Sci. Rep. 9 (2019) 13715, https://doi.org/10.1038/s41598-019-49900-9.

[68] W. Lee, G. Lim, S.H. Ko, Significant thermoelectric conversion efficiency enhancement of single layer graphene with substitutional silicon dopants, Nano Energy 87 (2021) 106188, https://doi.org/10.1016/j.nanoen.2021.106188.

[69] R. Beams, L. Gustavo Cançado, L. Novotny, Raman characterization of defects and dopants in graphene, J. Phys. Condens. Matter 27 (2015) 083002, https://doi.org/10.1088/0953-8984/27/8/083002.

[70] M. Politou, X. Wu, I. Asselberghs, A. Contino, B. Soree, I. Radu, C. Huyghebaert, Z. Tokei, S. De Gendt, M. Heyns, Evaluation of multilayer graphene for advanced interconnects, Microelectron. Eng. 167 (2017) 1–5, https://doi.org/10.1016/j.mee.2016.09.011.

[71] A. Krajewska, K. Oberda, J. Azpeitia, A. Gutierrez, I. Pasternak, M.F. López, Z. Mierczyk, C. Munuera, W. Strupinski, Influence of Au doping on electrical properties of CVD graphene, Carbon N Y 100 (2016) 625–631, https://doi.org/10.1016/j.carbon.2016.01.066.

[72] A.F. May, G.J. Snyder, Introduction to Modeling Thermoelectric Transport at High Temperatures, CRC Press, New York, 2012.
[73] M. Cutler, N.F. Mott, Observation of anderson localization in an electron gas, Phys. Rev. 181 (1969) 1336–1340, https://doi.org/10.1103/PhysRev.181.1336.
[74] E. Maciá-Barber, Thermoelectric Materials: Advances and Applications, Pan Stanford Publishing Pte. Ltd., 2015, https://doi.org/10.4032/9789814463539.
[75] X. Lu, S. Gu, S. Fan, X. Lu, J. Du, Y. Fan, Q. Zheng, L. Wang, W. Jiang, Enhanced thermoelectric composite performance from graphene nanosheets additives in $AgSbTe_2$ matrix, Ceram. Int. 48 (2022) 27891–27898, https://doi.org/10.1016/j.ceramint.2022.06.092.
[76] G.M. Guttmann, D. Dadon, Y. Gelbstein, Electronic tuning of the transport properties of off-stoichiometric PbxSn1-xTe thermoelectric alloys by Bi2Te3 doping, J. Appl. Phys. 118 (2015), https://doi.org/10.1063/1.4928459.
[77] S. Oh, B.J. Kim, J. Kim, Layer-by-layer AuCl3 doping of stacked graphene films, Phys. Status Solidi Rapid Res. Lett. 8 (2014) 441–444, https://doi.org/10.1002/pssr.201409085.
[78] N. Raveendran, T. Ghosh, V. Ignatious, V. Darshan, N. Jacob, B. Deb, C. Vijayakumar, Thermoelectric properties of self-assembled thiophene derivatives: effect of molecular structure on doping efficiency and Fermi level alignment, Mater. Today Energy 34 (2023), https://doi.org/10.1016/j.mtener.2023.101296.
[79] X. Shi, L. Chen, C. Uher, Recent advances in high-performance bulk thermoelectric materials, Int. Mater. Rev. 61 (2016) 379–415, https://doi.org/10.1080/09506608.2016.1183075.
[80] M. Rahimi, K. Sobnath, F. Mallet, P. Lafarge, C. Barraud, W. Daney de Marcillac, D. Fournier, M.L. Della Rocca, Complete determination of thermoelectric and thermal properties of supported few-layer two-dimensional materials, Phys. Rev. Appl. 19 (2023) 034075, https://doi.org/10.1103/PhysRevApplied.19.034075.
[81] M. Asgari, L. Viti, O. Balci, S.M. Shinde, J. Zhang, H. Ramezani, S. Sharma, A. Meersha, G. Menichetti, C. McAleese, B. Conran, X. Wang, A. Tomadin, A. C. Ferrari, M.S. Vitiello, Terahertz photodetection in scalable single-layer-graphene and hexagonal boron nitride heterostructures, Appl. Phys. Lett. 121 (2022), https://doi.org/10.1063/5.0097726.
[82] H.J. Hwang, S.-Y. Kim, S.K. Lee, B.H. Lee, Large scale graphene thermoelectric device with high power factor using gradient doping profile, Carbon N Y 201 (2023) 467–472, https://doi.org/10.1016/j.carbon.2022.09.048.
[83] R. Santhosh, R. Abinaya, J. Archana, S. Ponnusamy, S. Harish, M. Navaneethan, Controlled grain boundary interfaces of reduced graphene oxide in $Ag_2Se$ matrix for low lattice thermal conductivity and enhanced power factor for thermoelectric applications, J. Power Sources 525 (2022) 231045, https://doi.org/10.1016/j.jpowsour.2022.231045.
[84] Y. Bai, T. Ouyang, X. Li, W. Wang, Y. Yan, Z. Kong, X. Ma, Z. Li, Z. Li, X. Cai, J. Cai, H. Tan, Graphene oxide embedded in $Bi_2S_3$ nanosheets by hydrothermal method to enhance thermoelectric performance, Mater. Chem. Phys. 301 (2023) 127643, https://doi.org/10.1016/j.matchemphys.2023.127643.
[85] C. Gayner, R. Sharma, I. Malik, M. Kumar, S. Singh, K. Kumar, J. Tahalyani, T. Srivastava, K.K. Kar, H. Yokoi, A.K. Naskar, Enhanced thermoelectric performance of PbSe-graphene nanocomposite manufactured with acoustic cavitation induced defects, Nano Energy 94 (2022) 106943, https://doi.org/10.1016/j.nanoen.2022.106943.